Activation of Histone 3 Lysine 9 methyl writing and reading capabilities within the G9a-GLP heterodimer

Nicholas A Sanchez[1,2], Lena M Kallweit[1], Charles L Clemmer[1] and Bassem Al-Sady[1,*].

[1]Department of Microbiology &Immunology, George Williams Hooper Foundation, University of California San Francisco, San Francisco, CA 94143, USA, [2]TETRAD graduate program, University of California San Francisco, San Francisco, CA 94143, USA

[*]correspondence: bassem.al-sady@ucsf.edu

Unique among metazoan repressive histone methyltransferases, G9a and GLP, which target histone 3 lysine 9 (H3K9), require dimerization for productive H3K9 mono (me1)- and dimethylation (me2) *in vivo*. Intriguingly, even though each enzyme can independently methylate H3K9, the predominant active form *in vivo* is a heterodimer of G9a and GLP. How dimerization influences the central H3K9 methyl binding ("reading") and deposition ("writing") activity of G9a and GLP, and why heterodimerization is essential *in vivo* remains opaque. Here, we examine the H3K9me "reading" and "writing" activities of defined, recombinantly produced homo- and heterodimers of G9a and GLP. We find that both reading and writing are significantly enhanced in the heterodimer. Compared to the homodimers, the heterodimer has higher recognition of H3K9me2, and a striking ~ 10-fold increased k_{cat} for nucleosomal substrates under multiple turnover conditions, which is not evident on histone tail peptide substrates. This however is not encoded by altered nucleosome affinity, which is dominated by the G9a protomer and comparable across the homo- and heterodimer. Our results indicate that heterodimerization may be required to relieve autoinhibition of H3K9me reading and chromatin methylation evident in G9a and GLP homodimers. Relieving this inhibition may be particularly important in early differentiation when large tracts of H3K9me2 are deposited by G9a-GLP, which may require a more active form of the enzyme.

INTRODUCTION

The animal genome is partitioned into active and inactive regions by gene-repressive structures such as heterochromatin that restrict access to gene-activating factors (1). In early mammalian development, the genome of embryonic stem cells is highly transcriptionally active and features little heterochromatin marked by histone 3 lysine 9 methylation (H3K9me) (2). As differentiation begins, H3K9me heterochromatin expands, remodeling the genome and restricting fate (3). These expansions are carried out by the SETDB1 H3K9 trimethylase (me3) (3, 4) and the G9a and GLP H3K9 mono-and dimethylases (me1/me2). G9a and GLP direct the expansion of large tracks of H3K9me2, which can adopt a lineage-specific pattern (5). This heterochromatin expansion represses lineage inappropriate genes directly or silences enhancers that in turn direct several genes (6).

Like several heterochromatic methyltransferases, G9a and GLP have the capacity to both read and write H3K9me (7–10). Both enzymes contain an Ankyrin (ANK) repeat domain, which confers methyl-histone binding (reading) activity, and a SET domain, which confers methyltransferase (writer) activity. The presence of methylated substrates appears to stimulate G9a or GLP catalytic activity in an ANK domain-dependent manner (10). Other H3K9 methylases require such positive feedback for either lateral spreading (11, 12) or epigenetic maintenance (13, 14). How the ANK and SET domains of G9a and GLP regulate one another is opaque but may be central to understanding their function in cell fate control.

Unlike other metazoan H3K9 methyltransferases, G9a and GLP must associate with each other via their SET domains to carry out H3K9 methylation (9): When the interaction between the two enzymes is broken *in vivo*, the bulk of H3K9me1 and me2 is lost (15). This is despite the observation that each enzyme is individually capable of methylating histones *in vitro* (8–10, 16, 17). We hypothesized that forming the G9a-GLP complex (G9a-GLP) has a direct regulatory effect on the H3K9 methylation reaction. However, the biochemical and biophysical nature of homo- and heterotypic associations between G9a and GLP are poorly understood, as are any effects on H3K9me writing and reading that these associations may have.

In this study, we investigated the regulation heterodimerization imposes on G9a and GLP's ability to read and write H3K9me.

RESULTS

G9a and GLP form stable dimers at 1:1 stoichiometry

To directly assay the interplay between reading, writing, and dimerization, we expressed and purified G9a and GLP truncated to the C-terminal ANK and SET domains (ANK-SET), consistent with prior studies (10) (**Figure 1A**). To determine if G9a and GLP form homo- or heterodimers, we adopted a co-expression strategy: N-terminally 6xHis-tagged G9a (His:G9a) and N-terminally Maltose Binding Protein tagged GLP or G9a (MBP:GLP or MBP:G9a) were co-expressed in *E. coli*. Dimerization is assessed by a sequential affinity purification strategy from *E. coli* lysates. Sequential cobalt and amylose resin purification of either the His:G9a::MBP:G9a homomeric or His:G9a::MBP:GLP heteromeric complexes retains a dimer (**Figure 1B**). Quantification of SyPRO Red stained bands indicated dimerization at 1:1 stoichiometry for both complexes (**Figure 1B**). Consistent with this observation, MBP:G9a or MBP:GLP constructs expressed individually had similar retention profiles through size exclusion chromatography (data not shown). We examined the stability of G9a homo- and G9a-GLP heterodimers using a dilution-based assay, which assesses the off-rate of the complex. Each complex was diluted to 40nM (about 100 times) and allowed to dissociate for 1-2 hours at room temperature. We assessed dimer association by precipitating the His-tagged protein with cobalt resin and determining the fraction of MBP protein that remained bound. We observed little dissociation in either G9a homo or heterodimers (**SFigure 1**). To exclude the possibility that the N-termini of G9a or GLP counteract complex formation, we examined complex retention following sequential affinity purification of full-length proteins produced in insect cells. We found them to behave similarly to ANK-SET (**SFigure 2**). Together, these data indicate that G9a forms stable, 1:1 homodimers, as well as heterodimers with GLP.

For further characterization of the G9a-GLP heterodimer, we removed both the His and MBP tags by TEV-mediated proteolysis (**Figure 1C**). Using this "tagless" G9a-GLP molecule, we next ascertained the number of enzymes per complex. To do so, we determined its molecular weight using size exclusion chromatography (SEC) followed by multi-angle light scattering (MALS). We observed one major peak in our SEC-MALS measurement (**Figure 1D** left) and determined it to have a molecular weight of ~135 kDa **(Figure 1D**, right), roughly the theoretical molecular weight of our truncated G9a/GLP heterodimer (142 kDa). These data suggest that G9a-GLP is limited to a heterodimeric complex with one G9a and one GLP molecule.

Heterodimerization facilitates G9a and GLP binding to H3K9 methyl peptides

The presumably monomeric ANK domains of G9a and GLP have been shown to interact with both H3K9me1 and H3K9me2 histone tails, to largely similar extents (7, 10). Using fluorescence polarization, we asked whether the ability to engage H3K9me1/me2 is preserved in the dimeric ANK-SET molecule and whether heterodimerization affected this reading function (**Figure 2**). Interestingly, except for GLP ANK-SET binding

to me1 (**Figure 2A**), the presence of the SET domain in the context of homodimers is broadly inhibitory to H3K9me binding compared to published ANK alone data (7, 10). GLP ANK-SET has significantly reduced binding to me2 peptides (**Figure 2B**), while G9a ANK-SET has no discernable affinity for me1 and only slight affinity for me2 peptides (**Figure 2 C,D**). Heterodimerization abrogated the negative regulation imposed by the SET domain, allowing interaction with me1 and me2 peptides in a range comparable to the ANK domain alone (**Figure 2 E,F**). Taken together, these results suggest that within the ANK-SET homodimeric context, the ANK domains of both G9a and GLP are partially compromised in their ability to bind methyl peptides and that this inhibition is overcome upon heterodimerization.

Heterodimerization Stimulates G9a and GLP Catalytic Activity

Because dimerization occurs within the catalytic SET domain, we asked whether dimerization constitutively affects the methyltransferase activity of G9a-GLP. We determined Michaelis Menten kinetic parameters of G9a and GLP homodimers as well as the G9a-GLP heterodimer using an H3 histone tail peptide substrate ($H3_{1-20}$, (11)) (**Figure 3A**,**G**). While the K_M of all enzyme species were similar (e.g. **Figure 3B**) we observed changes of the k_{cat} within the heterodimer beyond those expected from equal contributions from G9a and GLP: The G9a and GLP k_{cats} on $H3_{1-20}$ are ~33min^{-1} and ~14min^{-1}, respectively. Rather than an intermediate value, G9a-GLP's k_{cat} is ~33min^{-1}, suggesting one or both enzymes are more active in the heterodimer than their respective homodimers. To determine which enzyme is stimulated in the heterodimer we made point mutations in either G9a (G9aS, Y1120V, Y1207F) or GLP (GLPS, Y1240F) abrogating their catalytic activity while still allowing dimerization with a wild type allele of their binding partner (15, 18). Comparing G9aS-GLP to GLP-GLP we observe that GLP's k_{cat} increased ~2 times upon heterodimerization (**Figure 3C**). Activity comparisons of G9a-GLPSET and G9a-G9a suggested no significant increase in activity of G9a in the heterodimer (data not shown), indicating that only GLP's activity is meaningfully enhanced in the heterodimer. Thus, these data imply a modest catalytic enhancement in G9a-GLP versus the homodimeric forms.

Next, we asked if the G9a-GLP heterodimer exhibits altered methylation kinetics on a mononucleosome, which mimics its cellular chromatin substrate (**Figure 3D**). We first measured Michaelis Menten parameters under multiple turnover conditions, just like for $H3_{1-20}$, for G9a-GLP and G9a-G9a on a reconstituted mononucleosome. In striking contrast to our observations on $H3_{1-20}$, G9a-GLP's k_{cat} is 10 times higher than that of G9a-G9a (**Figure 3E,G** and **SFigure 3B**). To further confirm this observation, and to additionally compare G9a-GLP to GLP-GLP, we performed methylation timecourses under near-saturating conditions for the mononucleosome, (5μM mononucleosome), as inferred from Michaelis-Menten curves in Figure 3E. Under these conditions, the heterodimer also exhibits higher activity (~ 8 times higher k_{cat}) than G9a-G9a. Similar to the $H3_{1-20}$ substrate, the GLP homodimer is the slowest enzyme construct of the three, preventing us from

producing a multiple turnover Michaelis-Menten curve. (**Figure 3F**). We conclude that the nucleosome substrate brings to fore the intrinsic catalytic differences between homo and heterodimers, revealing a dramatically increased k_{cat} for G9a-GLP. However, concomitant with this k_{cat} increase, we also noticed an increase in the nucleosome K_M for G9a-GLP (**Figure 3E,G**). This may indicate a decrease in binding affinity for the nucleosome but could also be due to other causes. To directly probe whether such an effect on the K_M indeed reflects differential substrate binding, we next directly probed nucleosome interactions.

The Heterodimer interacts with chromatin in a G9a specific manner.

As in the studies above with the H3 tail peptide, we used fluorescence polarization to measure the binding affinity of each ANK-SET dimer on a mononucleosome. For G9a-G9a and G9a-GLP homo- and heterodimers, respectively, we measure a similar K_d in the range of ~20μM (**Figure 4 A, B**), although we could not fully saturate this interaction given the limitations of ANK-SET protein production. As we can no longer measure this interaction for G9a in the context of a catalytically inactive SET domain (G9aS, **Figure 4C**), we believe these measurements reveal specific binding to the nucleosome, requiring the SET domain active site. These results have two implications: First, the apparent K_ds for G9a-G9a and G9a-GLP are similar, and not different by up to ~10 times as we observed for the nucleosome K_M (**Figure 3E**). Second, these K_ds are significantly larger than the corresponding K_Ms. These data suggest that the observed K_M differences are not a consequence of weaker substrate binding by G9a-GLP. Instead, they are consistent with the idea that product release is rate-limiting for nucleosomes, and that this limitation is more severe for G9a-G9a than G9a-GLP, resulting in a lower K_M.

GLP-GLP, unlike G9a-containing dimers, surprisingly, had a nearly immeasurable nucleosome affinity (**Figure 4D**). It is possible that in the heterodimer, GLP affinity is increased, allowing it to interact with chromatin to the same degree as G9a. To understand how GLP binding may be affected in the heterodimer, we measured its affinity for chromatin in the G9aS-GLP heterodimer (**Figure 4E**). In the heterodimer, GLP's affinity was only slightly increased. We conclude the G9a-GLP heterodimer makes initial contact with chromatin in a G9a-specific manner. We cannot exclude that GLP makes closer contact with the nucleosome in the heterodimer, but that GLPs contacts are dependent on, or stabilized, by wild-type G9a.

Finally, we examined whether our binding measurements reflected any interaction of G9a-GLP with nucleosomal DNA, a common feature of HMTs (11, 12). We compared fluorescence polarization of the Clr4 HMT to G9a-GLP on the 601 DNA (**SFigure 4A**) used to assemble our mononucleosomes. While we observe robust DNA binding for Clr4 to DNA consistent with prior work (19), we observed no binding of G9a-GLP, suggesting our nucleosome binding data solely reflect interaction with the histones (**SFigure 4B, C**). However,

DNA binding may be conferred by regions of G9a or GLP outside the ANK-SET module, in the protein N-terminus (**Figure 1A**).

DISCUSSION

Unusual among metazoan histone methyltransferases, G9a and GLP form dimers *in vivo* and this dimerization is essential for function (9). We discuss our findings regarding the ability of these proteins to 1. homo-and heterodimerize and the unanticipated consequences of heterodimerization on both H3K9me 2. reading, and 3. writing.

1. *Constitutive dimerization:* The degree to which dimerization, or the stability of dimers, is regulated by homo-and heteromeric associations is unknown. Our data argue that the ANK-SET portion of G9a and GLP homo- and heteromeric species form 1:1 dimers with low apparent dissociation and that efficient dimerization is not limited in the homomeric context (**Figure 1**, **SFigure 1**). However, *in vivo* experiments indicate that when G9a and GLP are present at equal cellular stoichiometry, the heterodimer is the preferred form and that homodimers can form when G9a or GLP is in excess (9). This *in vivo* preference may be due to regulation outside the ANK-SET domain. Taken together with our results, a picture emerges where G9a and GLP constitutively form homo- or heterodimers with relative pools determined by the steady-state accumulation of either protein. Homodimers, when formed, may then execute unique functions, for example in DNA repair for GLP (20), and in terminal muscle differentiation, where G9a and GLP control non-overlapping genes sets (21). We speculate that the heterodimer, with increased catalysis on chromatin and product recognition (below), is required when large domains of H3K9me1/2 are first formed and then maintained through cell division (6, 22), and that specialized and local chromatin methylation, or methylation of non-histone targets, may be carried out by homodimers.
2. *De-inhibition of H3K9me2 reading:* Our data suggest that H3K9me reading, in particular H3K9me2 is inhibited within the ANK-SET homodimer. As far as H3K9me reading, only the heterodimer appears capable of significant H3K9me2 recognition (**Figure 2)**, while both GLP-GLP and G9a-GLP can recognize H3K9me1. This differs from findings on the presumably monomeric G9a and GLP ANK domains alone as measured by fluorescence polarization (7) or ITC (10). Because the affinities we measure for H3K9me1/2 binding, where observed, are within 2-fold of these published affinities for ANK alone (7, 10), we do not believe that the ANK domains in our hands have lower specific activity. Instead, we interpret our data to indicate that either 1. inhibitory contacts between ANK and SET, or ANK and ANK across the two dimers are alleviated in G9a-GLP or 2. The heterodimerization interface induces a conformational change within the ANK. Beyond these interactions in the "naïve" state where the protein has not engaged substrate,

H3K9me ANK binding sites may be initially unavailable in the naïve protein but become fully available following initial nucleosome engagement. This could account for the observation of H3K9me1 or me2 specific stimulation of methylation by G9a and GLP homodimers on chromatin circles (10).

3. *Stimulation of chromatin methylation:* We observe both modest, constitutive activation of GLP on H3 tail peptides, and a dramatic increase in the k_{cat} towards nucleosomes compared to the homodimers. We believe two mechanisms can account for these results: 1. Relief of general autoinhibition. Like other histone methyltransferases, G9a and GLP may be limited by autoinhibition. The fission yeast Clr4 enzyme contains an autoinhibitory loop that is relieved by automethylation (23) and similar inhibitory loops have been shown for PRC2 and NSD1 (24, 25). The constitutive activation we observed in GLP upon heterodimerization (**Figure 3**) may be due to the restructuring of an autoinhibitory loop in the post-SET domain (26). Additional modes of active site activation may be present upon G9a-GLP engagement with the nucleosome. 2. Differential product release. Early experiments showed that G9a and GLP are significantly less active on chromatin than peptide or histone substrates (9), which we also observe here (**Figure 3G**), although peptide and nucleosome k_{cats} cannot be directly compared (methods). Intriguingly, G9a-G9a and G9a-GLP have lower K_Ms on nucleosomes compared to peptides (**Figure 3G**), which are in turn, surprisingly, lower than the K_ds (**Figure 4**). K_M>K_d conditions points to product release limiting the reaction on the nucleosome (27). The fact that G9a-G9a shows an up to 10 times lower K_M than G9a-GLP suggests that product release is less of a constraint for G9a-GLP, possibly due to different product interactions that "trap" the homodimer. Further investigation is required to determine the heterodimer-specific engagement with nucleosome substrate and product, as well as mechanisms of relief from inhibition.

The unique ability of the G9a-GLP molecule to recognize H3K9me2 as well as methylate chromatin, especially compared to the G9a homodimer (**Figure 4F**), begins to explain the strong requirement of the heterodimer for global maintenance of H3K9me2 and normal embryogenesis.

Methods

Purification of G9a/GLP Homo and Heterodimers.
To isolate the ANK-SET (10) G9a-GLP heterodimer, we coexpressed N-terminally tagged His:G9a and MBP:GLP from a single plasmid (QB3 Berkeley Macrolab expression vectors) in *E. coli* DE3 Rosetta cells and performed sequential cobalt- and amylose-charged resin affinity chromatography purification. Cells co-expressing His and MBP constructs were lysed on ice via sonication in lysis buffer (100mM Tris pH 8, 300mM NaCl, 10% glycerol (v/v), 0.1% Tween-20, with freshly added 1mM β-mercaptoethanol (BME), 1mM PMSF, 5mM Benzamidine, 200µM Leupeptin, Aproptinin, Pepstatin, Phenantroline). The clarified lysate was then bound to cobalt-charged resin (Takara) for 1hr and washed twice with lysis buffer. His tagged proteins were eluted with lysis buffer containing 400mM imidazole and bound immediately to amylose resin (NEB) for 1hr. MBP tagged proteins were eluted with lysis buffer + 20mM maltose. Affinity tags were then removed by incubation with 12mg TEV protease for 1hr at 25°C. TEV protease was absorbed to cobalt resin and the cleaved heterodimer was further purified by size exclusion chromatography (Superdex 200 Increase 10/300 column) and buffer exchanged into storage buffer (100mM Tris pH 8, 100mM KCl, 10% glycerol, 1mM $MgCl_2$, 20µM

$ZnSO_4$, 10mM BME). Homodimeric MBP:G9a or MBP:GLP ANK-SET constructs were purified as above, omitting the cobalt resin purification. All protein constructs were quantified using SDS page with BSA standards and Sypro Red stain.

Size-Exclusion Chromatography coupled to Multi Angle Light Scattering.
For size-exclusion, protein samples were injected at 10µM into a silica gel KW804 chromatography column (Shodex; Shanghai, China). For MALS, the chromatography system was coupled to an 18-angle light-scattering detector (DAWN HELEOS II, Wyatt Technology; Santa Barbara, CA) and a differential refractometer (Optilab-rEX, Wyatt Technology). Data collection was done at a flow rate of 0.4mL per minute. SEC MALS data were collected and analyzed using Astra 7 software (Wyatt technology; Santa Barbara, CA).

Preparation of mononucleosome substrates.
Histone proteins and nucleosomes were purified as described (28) with the following modifications: Following assembly nucleosomes were dialyzed overnight into storage buffer (above) or FP storage buffer (50mM HEPES pH 7.5, 100mM KCl, 10% glycerol) depending on the application. Dialyzed samples were concentrated using 10kda Millipore Sigma Amicon Ultra Centrifugal Filter Units. For fluoresnece poluzaiton, nucleosome were reconstited with a 5' fluosecented DNA template.

Methylation Assays.
All methylation reactions used a tritium-based assay to detect the methylated product. Substrate peptides or nucleosomes were mixed in a solution containing 9µM tritiated S-Adenosyl Methionine (SAM, Perkin Elmer) cofactor, and reactions were initiated upon addition of 0.4-0.8µM enzyme. Before adding enzyme, peptide reactions were supplemented with 1000µM cold SAM to fully saturate the SAM binding pocket (S Figure 3). Due to signal limitations, nucleosome reactions were not supplemented with SAM (see below). Reactions were run in 100mM Tris pH 8, 100mM KCl, 1mM $MgCl_2$, 20µM $ZnSO_4$, 10mM BME and quenched with laemmli buffer. Peptide reactions were performed as described (11). Mononucleosome methylation reactions were read out via autoradiography. Proteins were separated on a 18% SDS PAGE gel which was dried and exposed to a GE Phosphor screen for 72 hours along with a standard curve of tritiated SAM spotted on Whatman paper, and imaged on a STORM imager. Images were quantified using Image Quant software (Cytiva).

Kinetics.
All methylation reactions were performed under Multiple Turnover conditions (27). G9a and GLP each catalyze a two-substrate bi-bi reaction using the cofactor SAM and H3K9 as substrates (16). To determine initial rates, methylation time courses were traced at various concentrations of H3K9-containing substrate while keeping the concentration of SAM and enzyme constant. Plots of initial rate vs. concentration H3K9 substrate measured in duplicate or triplicate were fit to $V = Vmax*[S]/(K_M + [S])$ using Prism software to extract K_M and k_{cat} values as well as the 95% confidence interval bounds of the fit. For peptide reactions, we saturated the SAM binding pocket (see above) with a mixture of tritiated and non-tritiated SAM to measure kinetic parameters under pseudo first-order conditions. For nucleosome experiments, we could not fully saturate the SAM pocket, due to signal limitations. The k_{cat} values reported here are thus limited to second-order rate constants.

Fluorescence polarization.
Polarization assays with fluoresceinated $H3_{1-20}$ K9me1 or K9me2 peptides, 147bp 601 DNA template, and core nucleosomes were performed and K_d values estimated as described (11) with the following modifications: The reaction buffer was 100mM Tris pH 8, 100mM KCl, 1mM $MgCl_2$, 20uM $ZnSO_4$, 10mM BME, 0.1% NP-40. The concentration of peptides and nucleosomes was 150nM and 200nM for DNA. Polarization measurements were conducted on a Biotek Cytation 5 (peptide and nucleosome) or Molecular Devices Spectramax (DNA) plate reader with low volume plates (Corning) in either 10µl (peptide, nucleosome) or 40µl (DNA) total volume.

Acknowledgments.

We thank Carol A Gross and Danica Fujimori for thoughtful discussions and feedback. We thank the Southworth lab for training and access to the SEC-MALS equipment. N.A.S. was supported by a Hooper Graduate Student Fellowship, B.A-S. was supported by grants from the National Institutes of Health (DP2GM123484) and the UCSF Program for Breakthrough Biomedical Research (partially funded by the Sandler Foundation).

FIGURE LEGENDS

Figure 1: G9a and GLP form stable 1:1 homo- and heterodimers. **A.** Domain architecture of G9a-GLP. TOP: full-length enzymes. The C-terminus of G9a and GLP feature an automethylation residue (K), an acidic patch (E), and a cysteine-rich region (C). The N-termini contain ankyrin repeats (ANK) that bind H3K9me and a SET domain (SET) which is both the methylation catalytic domain and the dimerization interface (green circle). BOTTOM: Truncation ANK-SET construct used in this study. **B.** *E. coli* coexpression and purification strategy for identification of G9a homo and heterodimers. **C.** TEV cleavage of G9a-GLP heterodimers and purification via size exclusion chromatography **D.** SEC-MALS trace of G9a-GLP. LEFT: Full A280 (green) and Light Scattering (Red) traces. RIGHT: magnification of the main peaks with molecular weight determination (black). The measured molecular weight of the complex is 135kD (theoretical MW 142kD).

Figure 2: Heterodimerization facilitates G9a and GLP binding to H3K9 methyl peptides. Fluorescence Polarization measuring binding of H3K9 mono and dimethyl peptides to **A.&B.** GLP homodimers; **C.&D.** G9a homodimers; **E.&F**. G9a-GLP heterodimers. K_d values are indicated on plots. The 95% confidence interval (CI) is shown for fits with significant binding saturation (A., E., F). For curves with limited saturation and fits with wide range of K_d values, the lower bound of the 95% CI is shown.

Figure 3: Heterodimerization stimulates G9a and GLP catalytic activity. A. Reaction scheme of H3 tail peptide methylation. SAM cofactor was labeled with tritium (^{3}H)**. B.** Michaelis Menten fit of G9a-GLP heterodimer methylating H3 tail peptide. **C.** Michaelis Menten fit of GLP homodimer (purple) vs G9aS-GLP heterodimer (black). **D.** Reaction scheme of mononucleosome methylation reactions**. E.** Michaelis Menten fit of G9a-GLP heterodimer (green) and G9a homodimer (pink) methylating mononucleosomes. **F.** Initial rate comparison of G9a-GLP (green), G9a homodimer (pink), and GLP homodimer (purple) methylating mononucleosomes under saturating conditions. Reactions contained 10μM histone tails (5μM mononucleosome). **G.** Kinetic parameters for histone peptide and mononucleosome methylation. Values reflect kinetic parameters (upper value) and 95% confidence intervals (lower values) extracted from duplicate measurements. k_{cat}* for nucleosomes denotes a second order rate constant (see methods).

Figure 4: The G9a-GLP heterodimer interacts with the nucleosome in a G9a specific manner. Fluorescence polarization of mononucleosomes containing 147bp 601 DNA 5' fluorescein-labeled bound to **A.** G9a-GLP **B.** G9a-G9a **C.** Catalytically inactive G9aS-G9aS, **D.** GLP-GLP, **E.** G9aS-GLP. The 95% confidence interval (CI) is shown for fits with significant binding saturation (A., B.). For curves with limited saturation and fits with wide range of K_d values, the lower bound of the 95% CI is shown (D., E.). **F.** Model. G9a dimerizes with GLP to facilitate binding to H3K9me2 peptides and to stimulate methyltransferase activity on chromatin.

REFERENCES

1. Allshire, R. C., and Madhani, H. D. (2018) Ten principles of heterochromatin formation and function. *Nature reviews. Molecular cell biology*. **19**, 229–244
2. Percharde, M., Bulut-Karslioglu, A., and Ramalho-Santos, M. (2017) Hypertranscription in Development, Stem Cells, and Regeneration. *Dev Cell*. **40**, 9–21
3. Nicetto, D., and Zaret, K. S. (2019) Role of H3K9me3 heterochromatin in cell identity establishment and maintenance. *Current opinion in genetics & development*. **55**, 1–10
4. Nicetto, D., Donahue, G., Jain, T., Peng, T., Sidoli, S., Sheng, L., Montavon, T., Becker, J. S., Grindheim, J. M., Blahnik, K., Garcia, B. A., Tan, K., Bonasio, R., Jenuwein, T., and Zaret, K. S. (2019) H3K9me3-heterochromatin loss at protein-coding genes enables developmental lineage specification. *Science*. **363**, 294–297
5. Wen, B., Wu, H., Shinkai, Y., Irizarry, R. a, and Feinberg, A. P. (2009) Large histone H3 lysine 9 dimethylated chromatin blocks distinguish differentiated from embryonic stem cells. *Nature genetics*. **41**, 246–250
6. Zylicz, J. J., Dietmann, S., Gunesdogan, U., Hackett, J. A., Cougot, D., Lee, C., and Surani, M. A. (2015) Chromatin dynamics and the role of G9a in gene regulation and enhancer silencing during early mouse development. *eLife*. 10.7554/eLife.09571
7. Collins, R. E., Northrop, J. P., Horton, J. R., Lee, D. Y., Zhang, X., Stallcup, M. R., and Cheng, X. (2008) The ankyrin repeats of G9a and GLP histone methyltransferases are mono- and dimethyllysine binding modules. *Nature structural & molecular biology*. **15**, 245–50
8. Tachibana, M., Sugimoto, K., Nozaki, M., Ueda, J., Ohta, T., Ohki, M., Fukuda, M., Takeda, N., Niida, H., Kato, H., and Shinkai, Y. (2002) G9a histone methyltransferase plays a dominant role in euchromatic histone H3 lysine 9 methylation and is essential for early embryogenesis. *Genes & development*. **16**, 1779–91
9. Tachibana, M., Ueda, J., Fukuda, M., Takeda, N., Ohta, T., Iwanari, H., Sakihama, T., Kodama, T., Hamakubo, T., and Shinkai, Y. (2005) Histone methyltransferases G9a and GLP form heteromeric complexes and are both crucial for methylation of euchromatin at H3-K9. *Genes & development*. **19**, 815–26
10. Liu, N., Zhang, Z., Wu, H., Jiang, Y., Meng, L., Xiong, J., Zhao, Z., Zhou, X., Li, J., Li, H., Zheng, Y., Chen, S., Cai, T., Gao, S., and Zhu, B. (2015) Recognition of H3K9 methylation by GLP is required for efficient establishment of H3K9 methylation, rapid target gene repression, and mouse viability. *Genes & development*. **29**, 379–93
11. Al-Sady, B., Madhani, H. D., and Narlikar, G. J. (2013) Division of labor between the chromodomains of HP1 and Suv39 methylase enables coordination of heterochromatin spread. *Mol Cell*. **51**, 80–91
12. Muller, M. M., Fierz, B., Bittova, L., Liszczak, G., and Muir, T. W. (2016) A two-state activation mechanism controls the histone methyltransferase Suv39h1. *Nat Chem Biol*. **12**, 188–93
13. Ragunathan, K., Jih, G., and Moazed, D. (2015) Epigenetics. Epigenetic inheritance uncoupled from sequence-specific recruitment. *Science*. **348**, 1258699
14. Audergon, P. N., Catania, S., Kagansky, A., Tong, P., Shukla, M., Pidoux, A. L., and Allshire, R. C. (2015) Epigenetics. Restricted epigenetic inheritance of H3K9 methylation. *Science*. **348**, 132–5
15. Tachibana, M., Matsumura, Y., Fukuda, M., Kimura, H., and Shinkai, Y. (2008) G9a/GLP complexes independently mediate H3K9 and DNA methylation to silence transcription. *The EMBO journal*. **27**, 2681–90
16. Patnaik, D., Chin, H. G., Esteve, P. O., Benner, J., Jacobsen, S. E., and Pradhan, S. (2004) Substrate specificity and kinetic mechanism of mammalian G9a histone H3 methyltransferase. *The Journal of biological chemistry*. **279**, 53248–58
17. Chin, H. G., Pradhan, M., Esteve, P. O., Patnaik, D., Evans, T. C., and Pradhan, S. (2005) Sequence specificity and role of proximal amino acids of the histone H3 tail on catalysis of murine G9A lysine 9 histone H3 methyltransferase. *Biochemistry*. **44**, 12998–3006

18. Estève, P.-O., Patnaik, D., Chin, H. G., Benner, J., Teitell, M. A., and Pradhan, S. (2005) Functional analysis of the N- and C-terminus of mammalian G9a histone H3 methyltransferase. *Nucleic Acids Res*. **33**, 3211–3223
19. Akoury, E., Ma, G., Demolin, S., Bronner, C., Zocco, M., Cirilo, A., Ivic, N., and Halic, M. (2019) Disordered region of H3K9 methyltransferase Clr4 binds the nucleosome and contributes to its activity. *Nucleic acids research*. **47**, 6726–6736
20. Lu, X., Tang, M., Zhu, Q., Yang, Q., Li, Z., Bao, Y., Liu, G., Hou, T., Lv, Y., Zhao, Y., Wang, H., Yang, Y., Cheng, Z., Wen, H., Liu, B., Xu, X., Gu, L., and Zhu, W. G. (2019) GLP-catalyzed H4K16me1 promotes 53BP1 recruitment to permit DNA damage repair and cell survival. *Nucleic Acids Research*. **47**, 10977–10993
21. Battisti, V., Pontis, J., Boyarchuk, E., Fritsch, L., Robin, P., Ait-Si-Ali, S., and Joliot, V. (2016) Unexpected Distinct Roles of the Related Histone H3 Lysine 9 Methyltransferases G9a and G9a-Like Protein in Myoblasts. *Journal of Molecular Biology*. **428**, 2329–2343
22. Wen, B., Wu, H., Shinkai, Y., Irizarry, R. A., and Feinberg, A. P. (2009) Large histone H3 lysine 9 dimethylated chromatin blocks distinguish differentiated from embryonic stem cells. *Nature genetics*. **41**, 246–50
23. Iglesias, N., Currie, M. A., Jih, G., Paulo, J. A., Siuti, N., Kalocsay, M., Gygi, S. P., and Moazed, D. (2018) Automethylation-induced conformational switch in Clr4 (Suv39h) maintains epigenetic stability. *Nature*. **560**, 504–508
24. Bratkowski, M., Yang, X., and Liu, X. (2017) Polycomb repressive complex 2 in an autoinhibited state. *J Biol Chem*. **292**, 13323–13332
25. Graham, S. E., Tweedy, S. E., and Carlson, H. A. (2016) Dynamic behavior of the post-SET loop region of NSD1: Implications for histone binding and drug development. *Protein Sci*. **25**, 1021–1029
26. Wu, H., Min, J., Lunin, V. V., Antoshenko, T., Dombrovski, L., Zeng, H., Allali-Hassani, A., Campagna-Slater, V., Vedadi, M., Arrowsmith, C. H., Plotnikov, A. N., and Schapira, M. (2010) Structural biology of human H3K9 methyltransferases. *PLoS ONE*. 10.1371/journal.pone.0008570
27. Fersht, A. (1998) *Structure and Mechanism in Protein Science: A Guide to Enzyme Catalysis and Protein Folding*, 1st edition, W. H. Freeman, New York
28. Canzio, D., Chang, E. Y., Shankar, S., Kuchenbecker, K. M., Simon, M. D., Madhani, H. D., Narlikar, G. J., and Al-Sady, B. (2011) Chromodomain-mediated oligomerization of HP1 suggests a nucleosome-bridging mechanism for heterochromatin assembly. *Mol Cell*. **41**, 67–81

Supporting material:

Supporting Methods

Dilution Experiment
Purified His:G9a::MBP:GLP or His:G9a::MBP:G9a complexes were diluted to 40nM in lysis buffer and allowed to dissociate for 1-2hr at room temperature in a volume of 20µL. 7µL cobalt-charged resin was added to each sample and incubated for 30min to allow resin binding. The resin was washed twice with lysis buffer and 20µL 1x Laemmli Buffer was then added to resin. The ratio of MBP tagged protein to his tagged protein was assessed via SDS page with BSA standards and Sypro Red stain. Fraction assembled was =1 for a "stock protein" (SP) control that was not put through this assay and had a concentration of >4µM.

Insect Cell Expression
Bacculovirus containing full-length His:G9a and STREP:GLP co-expression cassettes (QB3 Berkeley Macrolab) were used to infect Sf9 cells (Expression Systems, Davis, California) grown in ESF921 media. Cells were infected for 72hr at an MOI of 0.1. Infected cells were flash frozen and stored at -80°C until thawed for purification. Cells were lysed on ice via sonication in lysis buffer (100mM Tris pH 8, 300mM NaCl, 10% glycerol (v/v), 0.1% Tween-20, with freshly added 1mM β-mercaptoethanol (BME), 1mM PMSF, 5mM Benzamidine, 200µM Leupeptin, Aproptinin, Pepstatin, Phenantroline). The clarified lysate was then bound to streptactin superflow resin (IBA) for 1hr and washed twice with 100mM Tris pH 8, 750mM NaCl, 10% glycerol (v/v), 0.1% Tween-20, freshly added 1mM BME. Strep tagged proteins were eluted with lysis buffer containing 5mM desthiobiotin and bound immediately to cobalt-charged resin (Takara) for 1hr. His tagged proteins were eluted with lysis buffer + 400mM imidazole. Complex formation was assessed via western blot.

Electromobility Shift Assay
To assess binding to 601 DNA via EMSA, G9a-GLP or Clr4 were incubation with 200nM of a 147bp 601 DNA template in 50mM HEPES pH 7.5, 100mM KCl, 10% glycerol, 0.1% NP-40 in a 10µL volume. Upon mixing, 50% glycerol was added to 5% final and samples were run on a 5% Tris-Glycine Native Gel. Samples were imaged using Chemidoc MP Imaging System (Biorad).

Supporting Figure 1: Stability of G9a-G9a and G9a-GLP complexes through a dilution assay. A. Experiment scheme. His:G9a coexpressed with either MBP:G9a or MBP:GLP was purified by sequential affinity purification as in Figure 1. The complexes were diluted and kept at 25°C for 1-2hrs. After this incubation, His:G9a was isolated via cobalt resin precipitation. **B.** The relative amount of His and MBP tagged proteins retained after cobalt resin precipitation was quantified by SyPRO Red staining and normalized to a stock protein (SP, > 4µM) of purified undiluted protein (fraction associated). The highest dilution for G9a-G9a and G9a-GLP, 40nM or > 100 times dilution, is shown.

Supporting Figure 2: Full-length G9a and GLP purify as a heterodimer from insect cells. A. Full-length GLP and G9a were N-terminally tagged with a STREP or 6XHis tag, respectively, co-expressed from a baculoviral construct in Sf9 insect cells, and isolated by sequential STREPTACTIN (Tactin) and Cobalt (Co^{2+}) affinity resins. **B.** Western blots of baculovirus-infected or uninfected Sf9 lysates (LEFT) or affinity resin eluates (RIGHT) with anti-His tag or anti-STREP tag antisera. The single-channel and merged images are shown.

Supporting Figure 3: S-adenosyl methionine K_M and G9a-G9a mononucleosome Michaelis Menten kinetics. A. The K_M for SAM was determined with G9a-GLP and $H3_{1-20}$ peptide substrates. Initial rates are plotted at indicated total SAM concentrations and the curve fit to $V = Vmax*[S]/(K_M + [S])$. **B.** A magnification of Michaels-Menten fit for G9a-G9a Multiple Turnover kinetics as shown in Figure 3E.

Supporting Figure 4: G9a-GLP does not bind DNA. A. G9a-GLP heterodimer or the monomeric fission yeast Clr4 H3K9 methyltransferase were assessed for binding the fluorescein-labeled 147bp "601" mononucleosome DNA template. **B.** Electro-Mobility shift Assay with G9a-GLP or Clr4 at indicated concentrations. **C.** Fluorescence polarization assay with G9a-GLP or Clr4 at indicated concentrations.

Figure 1

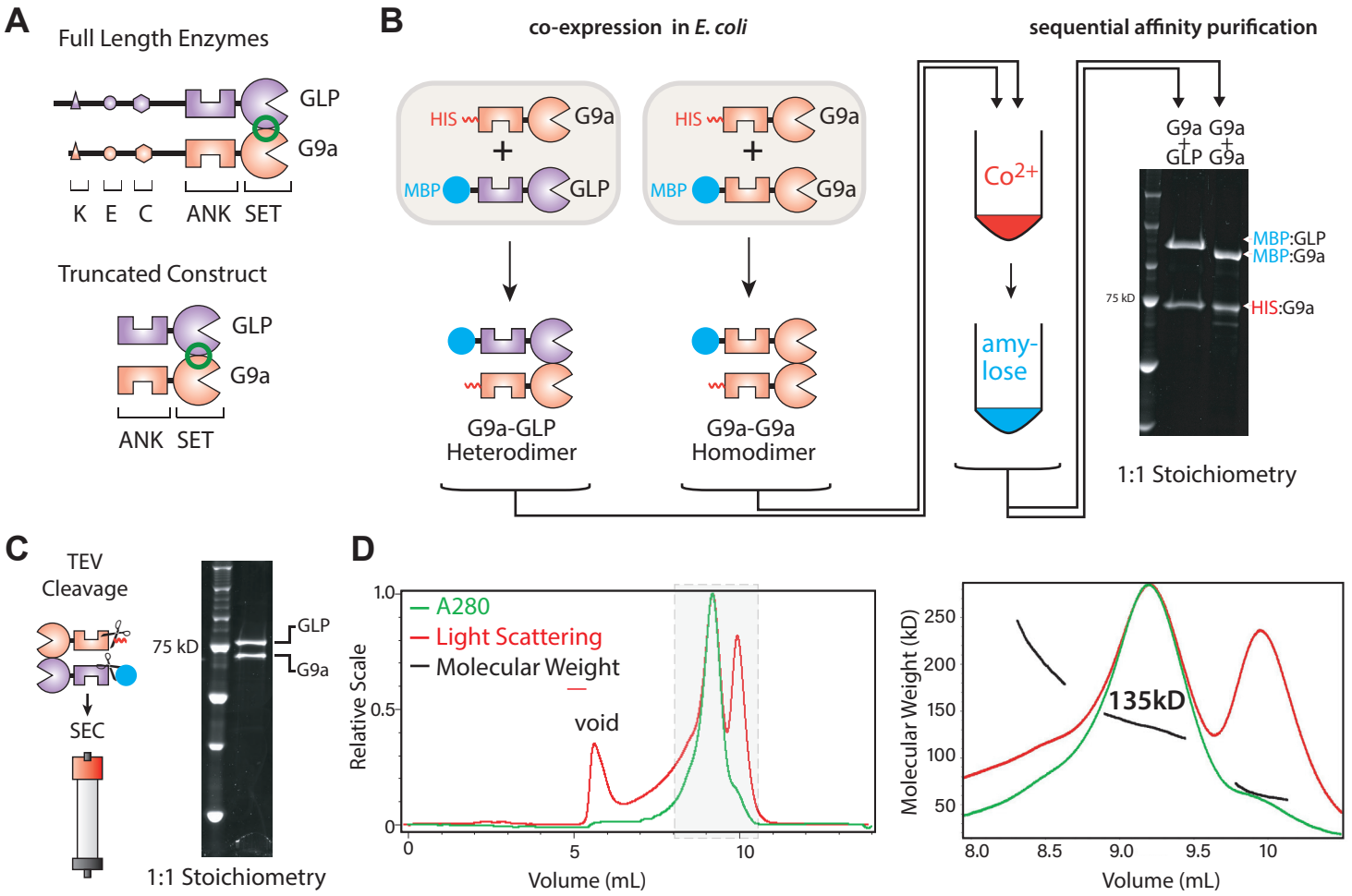
A
Full Length Enzymes
GLP
G9a
K E C ANK SET
Truncated Construct
GLP
G9a
ANK SET
B
co-expression in E. coli
sequential affinity purification
HIS
G9a
MBP
GLP
HIS
G9a
MBP
G9a
G9a-GLP Heterodimer
G9a-G9a Homodimer
Co2+
amy-lose
G9a G9a
+ +
GLP G9a
MBP:GLP
MBP:G9a
HIS:G9a
75 kD
1:1 Stoichiometry
C
TEV Cleavage
SEC
75 kD
GLP
G9a
1:1 Stoichiometry
D
A280
Light Scattering
Molecular Weight
void
Relative Scale
1.0
0.5
0
0
5
10
Volume (mL)
Molecular Weight (kD)
250
200
150
100
50
135kD
8.0
8.5
9.0
9.5
10
Volume (mL)

Figure 2

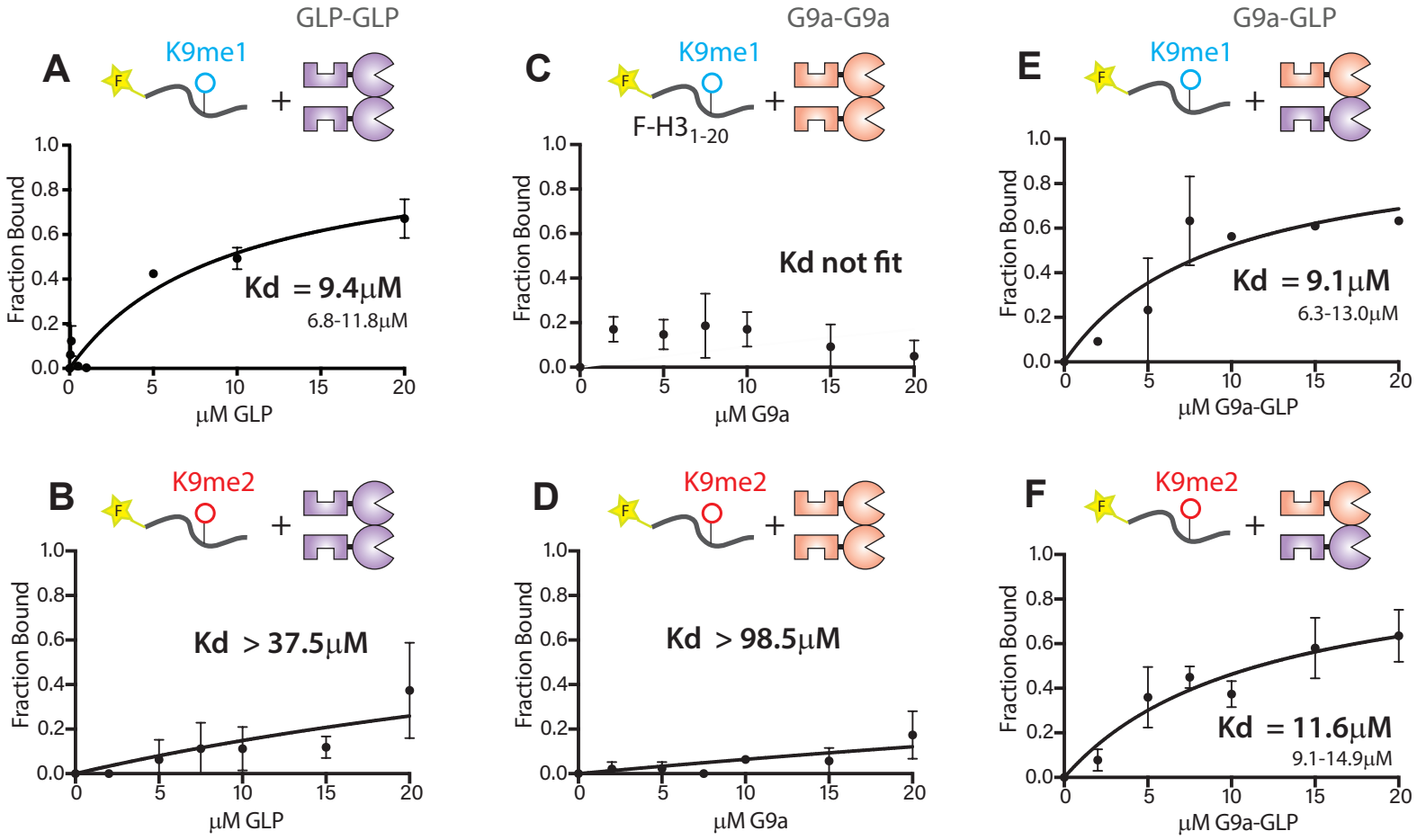
GLP-GLP
A
K9me1
Fraction Bound
Kd = 9.4μM
6.8-11.8μM
μM GLP
B
K9me2
Kd > 37.5μM
μM GLP
G9a-G9a
C
K9me1
F-H3 1-20
Kd not fit
μM G9a
D
K9me2
Kd > 98.5μM
μM G9a
G9a-GLP
E
K9me1
Kd = 9.1μM
6.3-13.0μM
μM G9a-GLP
F
K9me2
Kd = 11.6μM
9.1-14.9μM
μM G9a-GLP

Figure 3

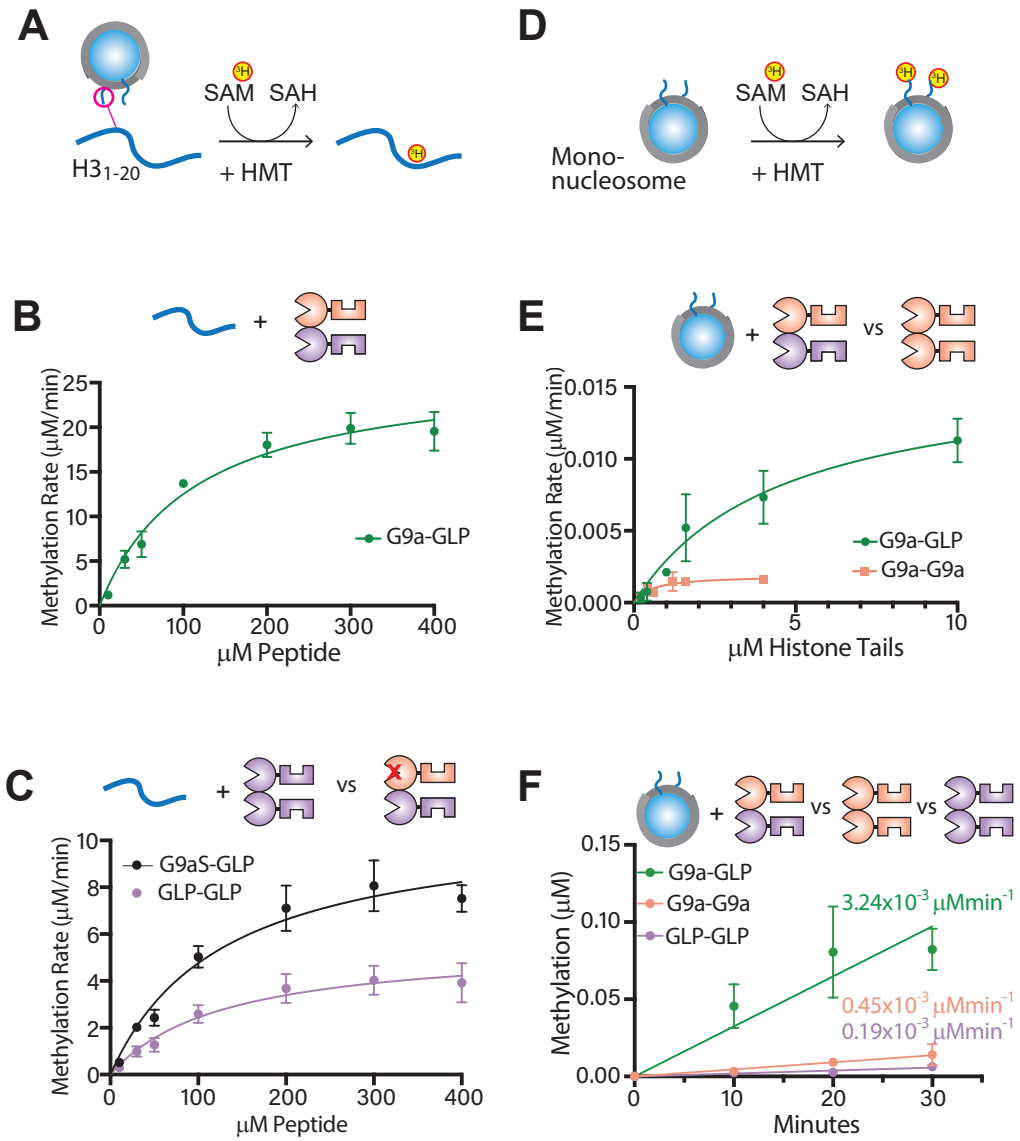

G

dimer	H3 1-20 peptide k_{cat} (min^{-1})	H3 1-20 peptide K_M (μM)	core nucleosome k_{cat}* (min^{-1})	core nucleosome K_M (μM)
G9a-G9a	32.6 24.6-34.6	133.6 86.6-212.5	0.0047 0.0034-0.0067	0.54 0.18-1.4
GLP-GLP	14.0 9.5-15.5	128.6 72.2-244.2	N/A	N/A
G9a-GLP	33.5 26.0-34.5	114.1 77.8-170.9	0.041 0.029-0.072	4.6 2.0-13.3
G9aS:-GLP	27.2 20.5-28.3	128.1 80.3-211.6	N/A	N/A

Figure 4

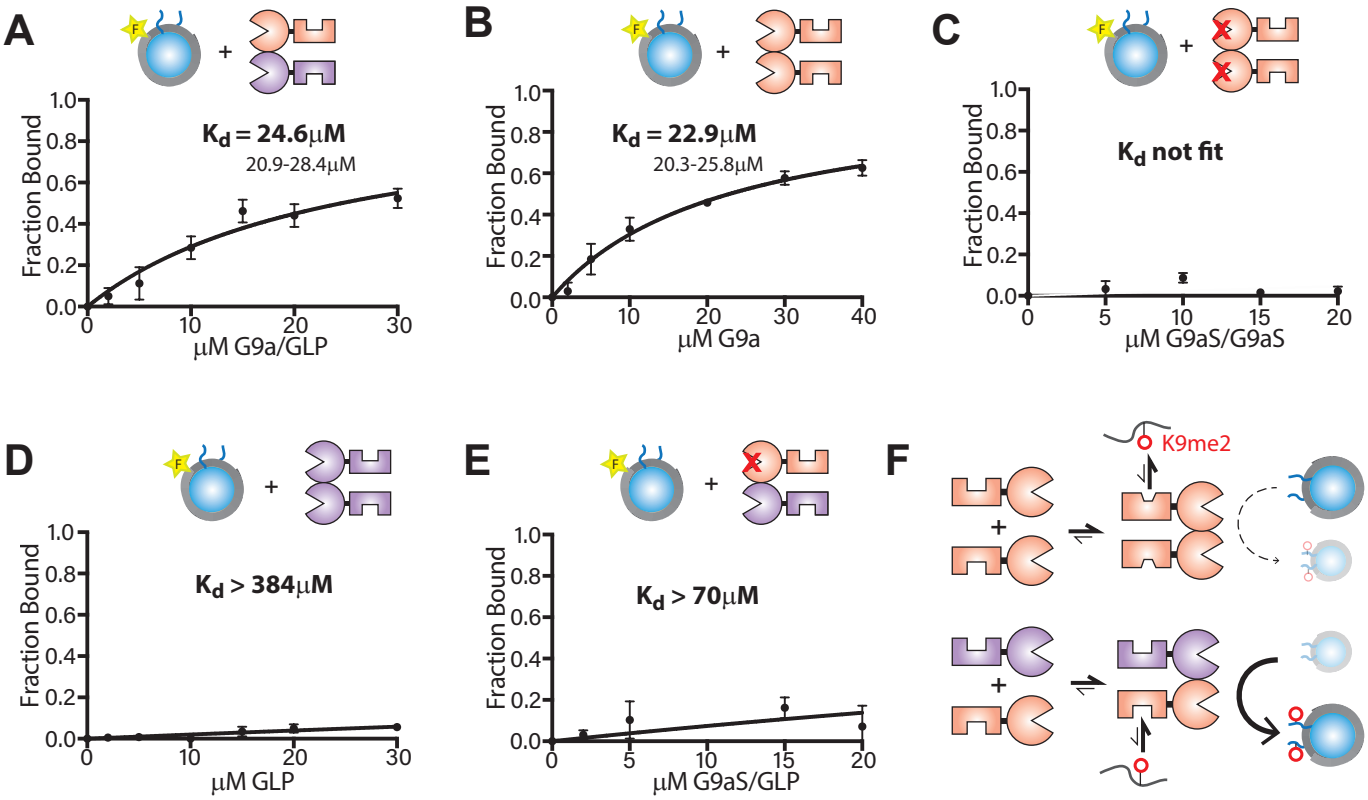
A
Fraction Bound
K_d = 24.6μM
20.9-28.4μM
μM G9a/GLP
B
Fraction Bound
K_d = 22.9μM
20.3-25.8μM
μM G9a
C
Fraction Bound
K_d not fit
μM G9aS/G9aS
D
Fraction Bound
K_d > 384μM
μM GLP
E
Fraction Bound
K_d > 70μM
μM G9aS/GLP
F
K9me2

Supporting Figure 1

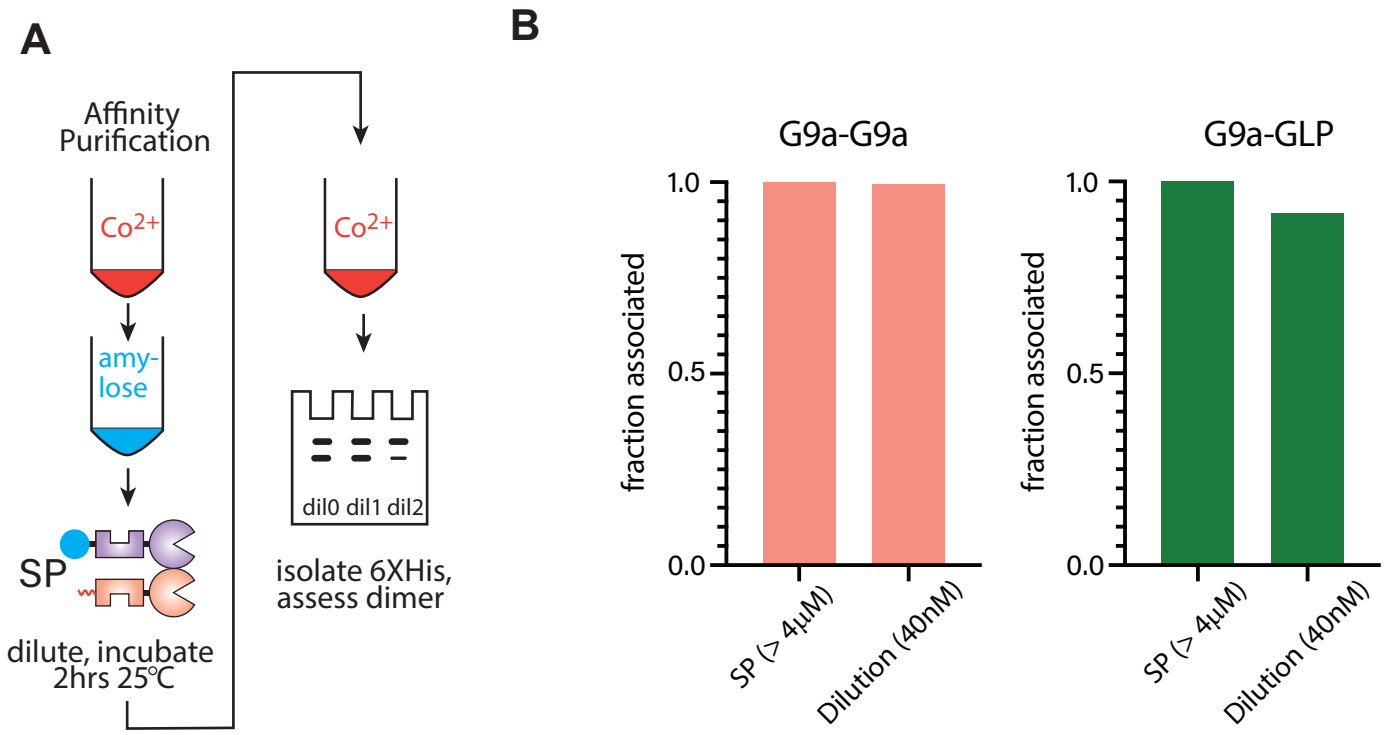

Supporting Figure 2

A

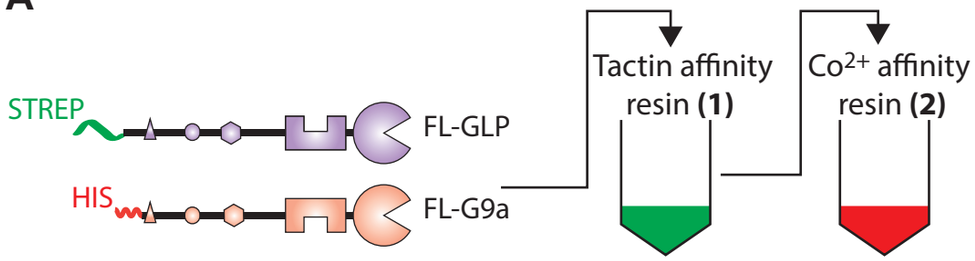

B

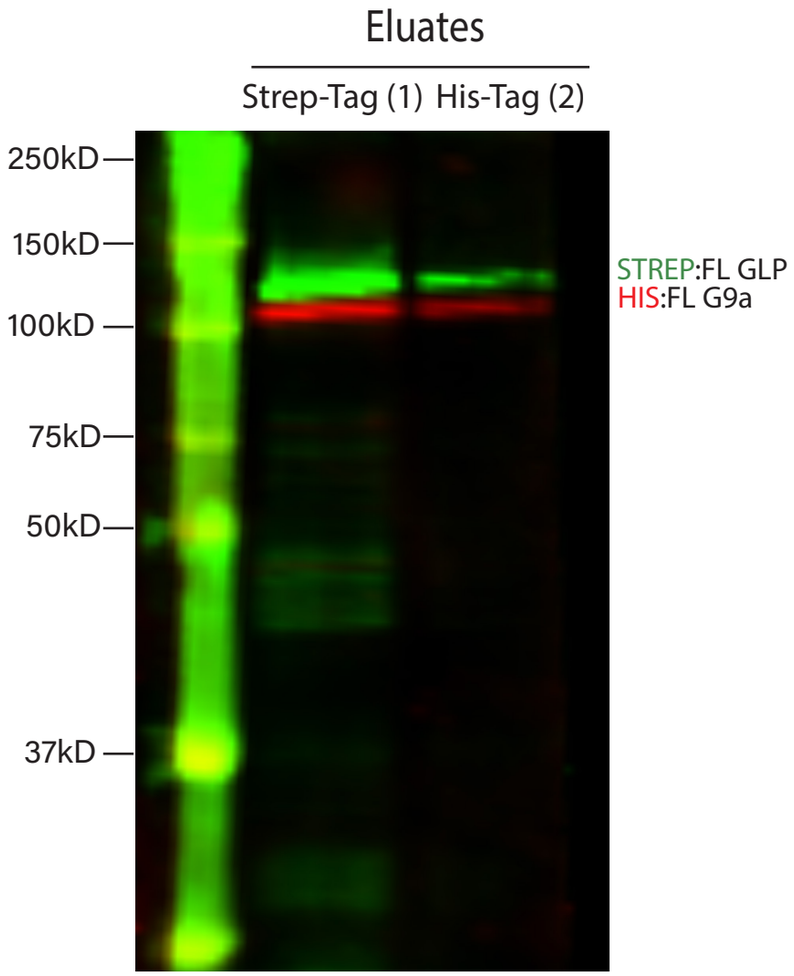

Supporting Figure 3

A

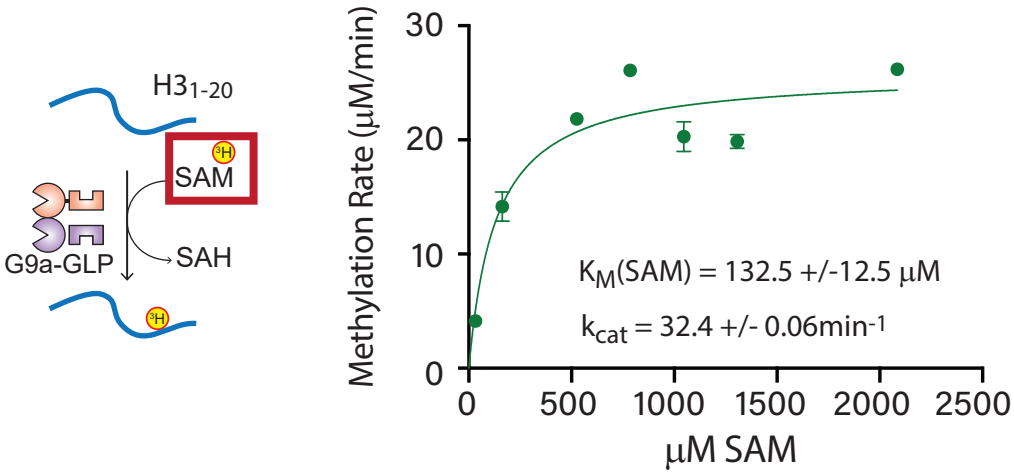

B

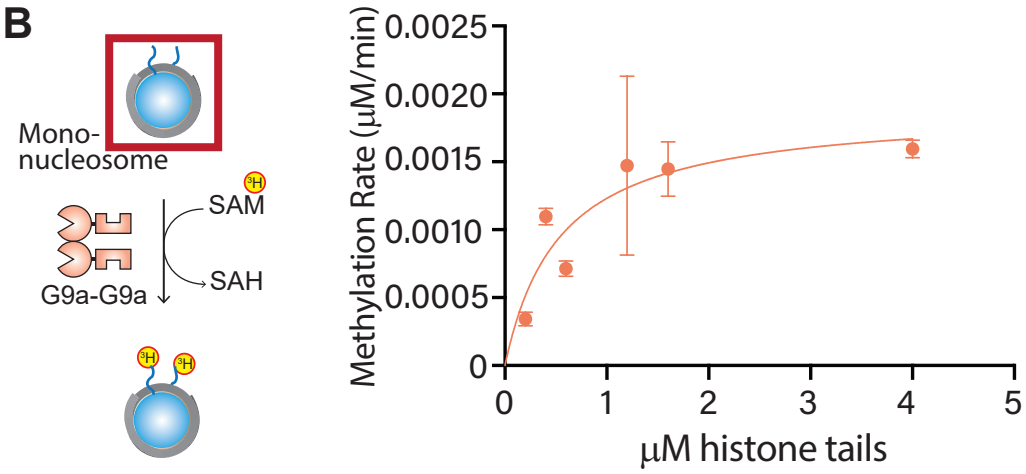
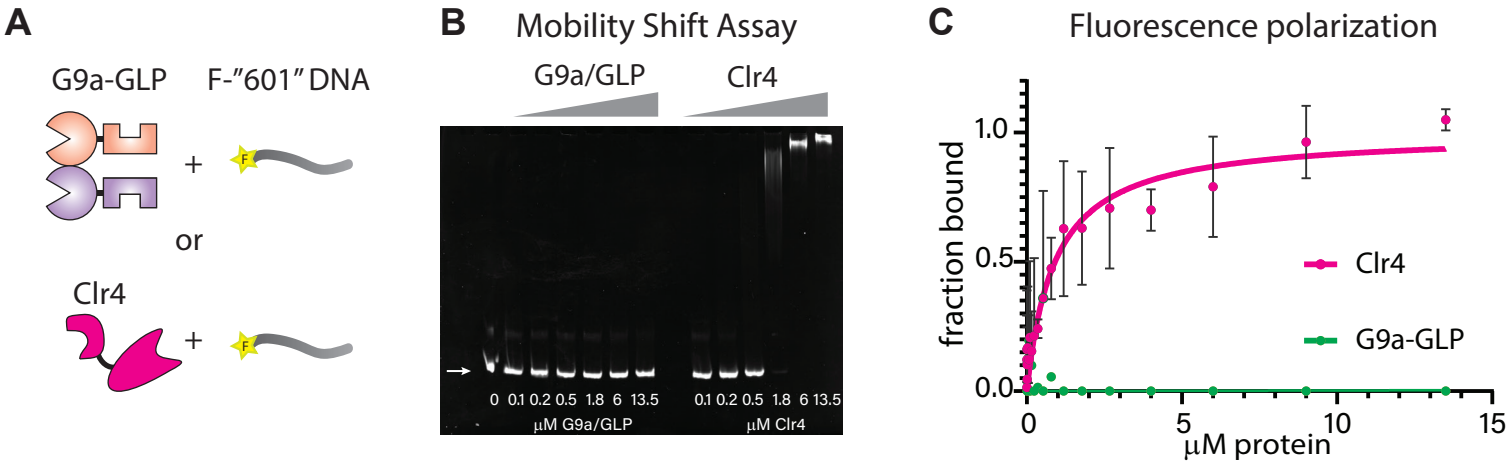
Supporting Figure 4